Journal of Nuclear Materials 405 (2010) 244–251

Contents lists available at ScienceDirect

Journal of Nuclear Materials

journal homepage: www.elsevier.com/locate/jnucmat

Surface desorption and bulk diffusion models of tritium release from Li_2TiO_3 and Li_2ZrO_3 pebbles

R.E. Avila [a,*], L.A. Peña [b], J.C. Jiménez [b]

[a] Departamento de Materiales Nucleares, Comisión Chilena de Energía Nuclear, Cas. 188-D, Santiago, Chile
[b] Departamento de Producción y Servicios, Comisión Chilena de Energía Nuclear, Cas. 188-D, Santiago, Chile

ARTICLE INFO

Article history:
Received 1 September 2009
Accepted 13 August 2010

ABSTRACT

The release of tritium from Li_2TiO_3 and Li_2ZrO_3 pebbles, in batch experiments, is studied by means of temperature programmed desorption. Data reduction focuses on the analysis of the non-oxidized and oxidized tritium components in terms of release limited by diffusion from the bulk of ceramic grains, or by first or second order surface desorption. By analytical and numerical methods the in-furnace tritium release is deconvoluted from the ionization chamber transfer functions, for which a semi-empirical form is established. The release from Li_2TiO_3 follows second order desorption kinetics, requiring a temperature for a residence time of 1 day (T_{1dRes}) of 620 K, and 603 K, of the non-oxidized, and the oxidized components, respectively. The release from Li_2ZrO_3 appears as limited by either diffusion from the bulk of the ceramic grains, or by first order surface desorption, the first possibility being the more probable. The respective values of T_{1dRes} for the non-oxidized component are 661 K, according to the first order surface desorption model, and 735 K within the bulk diffusion limited model.

1. Introduction

The release of tritium (T) from neutron irradiated lithium ceramics is a major concern towards the operation of fusion reactors, as it determines the tritium retention within the ceramic during and after operation [1]. Current interest, as regards Li-ceramics is focused [2] on Li_2TiO_3 and Li_4SiO_4 pebbles, and Li_2ZrO_3 was strongly considered for some time.

This topic has been the object of various studies, mainly, by means of in-core, continuous cycle irradiation-release experiments [3,4], and by sealed capsule irradiation, followed by out-of-pile release under controlled temperature and purge gas conditions [5] (batch experiments). The experiments in the present work have been conducted in the second fashion.

The analysis of release experiments has focused on establishing either surface desorption or bulk diffusion as the limiting release process, and on identifying either first or second order as the surface desorption kinetics. However, the processes by which T moves from the bulk of the ceramic grains to the surface, and desorbs, are certainly much more involved than those simple concepts, an elaborate modeling [6] approach being available for the purpose. In particular, crystalline defects have been proposed [7] as T trapping sites, the annihilation of which may control the T release. In that perspective, the observation of first or second order release kinetics would reveal that of the crystalline defect annihilation. Diffusion controlled release could still follow if the kinetics of detrapping are much faster than diffusion.

Nonetheless, the simple bulk diffusion or surface desorption limited release models are instrumental to the overall description of the release process, for the design of a T breeder first wall in a fusion reactor, in particular. In that direction, a description of the temperature dependence of the T residence time, defined as the T inventory divided by the release rate, is critical. Thus, in this work, the temperature of the T breeding blanket required for a residence time of 1 day will be used as a benchmark value.

The present work contributes the contrast of the release rates from Li_2TiO_3 vs. that from Li_2ZrO_3, and the application of analytical and numerical analysis methods to temperature programmed desorption (TPD) experiments. Careful attention is paid to recovering the in-furnace release curve, from the signals spread to higher temperature which result from the use of ionization chambers to monitor the T activity within the carrier gas stream.

2. The experiments

Li_2TiO_3 pebbles (provided by collaborators [8] at our home institution) were synthesized by solid state reaction of Li_2CO_3, and TiO_2 at 1173 K, followed by grinding, spheronization of the

Abbreviations: IC, ionization chamber; SD*n*, surface desorption of order *n*; BLR, bulk limited release; LFEP, low frequency error power average or average of the power spectrum (of the error) up to a frequency of 0.008.

* Corresponding author.
E-mail address: ravila@cchen.cl (R.E. Avila).

0022-3115/$ - see front matter © 2010 Elsevier B.V. All rights reserved.
doi:10.1016/j.jnucmat.2010.08.009

powder, and pebble sintering at 1473 K. Relevant morphological characteristics of the Li_2TiO_3 pebbles are: density 90.7% of theoretical density (td), grain size ($2b$) = 5 μm, pebble diameter: 0.5–0.8 mm, ligand: Natrosol, of which 2% is retained in the pebbles.

Commercial Li_2ZrO_3 pebbles, proprietary Lot 54101-B-2, from Cerac, Inc., Milwaukee, WI, USA, were kindly provided by Dr. Masabumi Nishikawa of the Graduate School of Engineering Science, Kyushu University, Japan. The Li_2ZrO_3 pebbles are 1 mm in diameter, grain size ($2b$) = 13 μm, density 91.4% td. According to Casadio et al. [9] the size difference between the Li_2TiO_3 and Li_2ZrO_3 pebbles should not affect the release behavior, which is determined mainly by the microstructure.

The powder from pellets ground by hand, in an agate mortar, were analyzed by X ray diffraction (Fig. 1) using a Siemens D5000 diffractometer, in the θ–θ configuration, with Cu Kα radiation, at 40 kV, 20 mA, and graphite monochromator. The diffractogram of Li_2TiO_3 pellets shows this material is fully crystalline, in the monoclinic base centered (S.G. C2/c) structure (PDF 0-33-0831). The analysis of the commercial Li_2ZrO_3 pebbles shows an amorphous component, as well as other phases than Li_2ZrO_3. Thus, a quantitative analysis was made, by addition of NIST 676a alumina standard, indicating that only 33% of the powder is crystalline. Within the crystalline fraction, 88% is monoclinic base centered Li_2ZrO_3 (PDF 1-076-1150), 8.2% is lithium carbonate (Li_2CO_3, PDF 01-087-0729), and 3.8% is best fit by zirconium oxide ($Zr_{0.932}O_2$, PDF 1-081-1315).

The pebble microstructure of both materials was examined by scanning electron microscopy (Jeol JSM 5410, with EDX capability), as shown in Fig. 2, where the pebble interior is displayed by fracturing in an agate mortar. Both materials display a compact arrangement, with grains 2–3 times larger in the Li_2ZrO_3 pebble than in the Li_2TiO_3 pebble. However, the amorphous component revealed by the XRD analysis suggests that the Li_2ZrO_3 grains contain a considerable fraction of amorphous material. Micropores are evident in both materials, as well as what appears as inner cavities which have been split open by the pebble fracture.

The energy dispersive analysis of both materials confirmed the absence of chemical contamination.

Before irradiation, the pebbles were prepared in quartz ampoules, by drying in vacuum (2 Pa or better) at temperature of 700–750 K, for 4 h. Then, the ampoules were sealed and placed in aluminum canisters, as it will be detailed at the beginning of Section 4. The in-core irradiation was carried out at thermal neutron flux

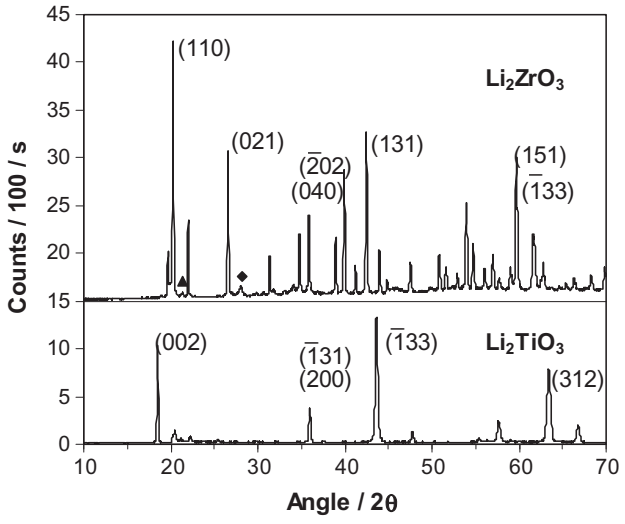

Fig. 1. X ray diffraction patterns of the Li_2TiO_3 and Li_2ZrO_3 pebbles, the latter displaced, upwards, for clarity. In the top trace, the triangle, and the diamond signal the main Li_2CO_3, and ZrO_2 peaks, respectively.

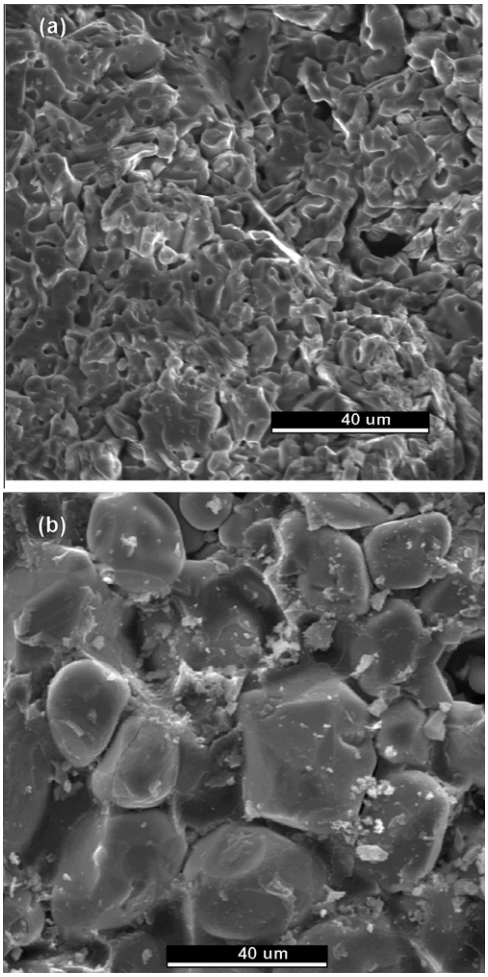

Fig. 2. Microstructure of (a) Li_2TiO_3 and (b) Li_2ZrO_3 pebbles.

between 2 and 3.4 · 10^{19}/m^2/s for time lapses in the 20–24 h range. In a 24 h irradiation, the degree of ^{6}Li burn-up is calculated at 0.24%. The ensuing damage, has been calculated considering the full collision cascades [10] from ^{3}H and ^{4}He reaction products. Displacement energies of 25 eV are assumed for Li and Ti, and 28 eV for O, leading to ~209 vacancies per $n(^6\text{Li}, ^3\text{H})^4\text{He}$ reaction, which imply ~1.25 displacements per atom (dpa) during a 24 h irradiation. These values of burn-up and damage imply that these experiments pertain to the starting ceramic conditions, as compared to irradiation in high flux fission reactors, or in a future fusion reactor.

The tritium (T) release experiments were conducted in a CRETE type of system built by AECL Research [11]. The procedure starts by breaking the quartz ampoules and dropping its contents into a furnace. The T released is swept at 100 sccm (standard cm^3/min) by a 0.1% H_2/He mixture, which is pre-humidified by bubbling, at 10 sccm, through distilled water, at room temperature. The carrier gas flows through the furnace towards a 200 ml ionization chamber (IC-1), followed by two ethylene glycol bubblers (to trap water), a molecular sieve filter, and a second ionization chamber (IC-2, same size as IC-1). Thus, the IC-1 signal represents the total T activity, while IC-2 represents the molecular hydrogen form.

Systems similar to the one described here have been used at several laboratories. Differences may include the immediate reduction of any oxidized tritium, before analysis, to avoid trapping of tritiated water at the ionization chamber. Also, the ionization chambers may be substituted with proportional counters. With slight modifications, the data analysis in the next section would easily apply to those variations of the analytical instrumentation.

The TPD experiments were carried out at heating rates from one, to 10 K/min up to1003 K, followed by a 30 min isotherm, followed by uncontrolled cooling. A microcomputer provides for the continuous recording of the furnace temperature, using K-type thermocouples, and the current signal (Keithley 617 electrometers) from each ionization chamber.

3. Analysis of TPD curves

3.1. System response deconvolution

The tritium activity signal, $a_1(t)$, and $a_2(t)$, measured by the ionization chambers IC-1 and IC-2, respectively, represents the total, $A_1(t)$, and non-oxidized, $A_2(t)$, T activities released from the furnace, delayed and smoothed by the transport of the gas mixture through the gas lines, IC's, bubblers, and molecular sieve filter. These distortions may be backtracked by recognizing $a_1(t)$ and $a_2(t)$ as the convolution of the corresponding initial activity with the unit step response functions, $r_i(t)$, of the furnace-to-IC-i system,

$$a_i(t) = r_i \otimes A_i = \int_0^t r_i(t-t')A_i(t')dt' \tag{1}$$

The system response functions have been modeled by assuming immediate mixing within the IC's, and bubblers, and simple time delays (without mixing) along the gas lines and molecular sieve filter.

The convolution expression (1) can be inverted by means of discrete fast Fourier transforms, relying on the property that $F\{f \otimes g\} = F\{f\}F\{g\}$, F denoting the Fourier transform operation. Thus,

$$a = F^{-1}\{F\{a_i\}/F\{r_i\}\}. \tag{2}$$

Mixing within the ionization chambers leads to

$$r(t) = \tau^{-1}\exp(-t/\tau) \tag{3}$$

where the time constant, τ, is the input flux divided by the chamber volume. More complex response functions are easily built using the commutativity and associativity properties of the convolution operation. Thus, if only the gas mixing at the two IC's is considered, and if the IC's have the same volume, ($\tau_1 = \tau_2 = \tau_m$), the signal from IC-2 is the double convolution:

$$a_2(t) = r(t) \otimes [r(t) \otimes a(t)] = [r(t) \otimes r(t)] \otimes a(t), \tag{4}$$

namely,

$$r_2(t) = (t/\tau_m^2)\exp(-t/\tau_m) \tag{5}$$

Considering additional convolutions at the gas bubblers, with time constants τ_m, and τ_b at the two IC's and two bubblers, respectively, the furnace to IC-2 response function is

$$r_2(t) = (B^2/A^3)\exp(-(1/\tau_m + 1/\tau_b)t)[(At + 2B)\exp(t/\tau_m) + (At - 2B)\exp(t/\tau_b)] \tag{6}$$

where $A = \tau_m - \tau_b$, $B = \tau_m\tau_b$, $\tau_m \neq \tau_b$. If $\tau = \tau_m = \tau_b$, the simpler expression $r_2(t) = (t^3/6)\exp(-t/\tau)$ results.

In practice, for the following section, Eq. (3) has been used for the response of the first ionization chamber. Next, an experimental form, $r_{1-2}(t)$, has been determined for the system response from IC-1 to IC-2. For this purpose, an activity pulse, from a T in He standard has been fed through the analysis system, and the signals $a_1(t)$, $a_2(t)$ have been recorded. Then, Eq. (2) has been inverted for r_{1-2}, with a_2 in place of a_i, and a_1 in place of a. This two stage approach to the deconvolution of the IC-2 signal allows for a more stable numerical procedure, than the use of Eq. (6).

The deconvolution operation, yielding $A_i(t)$, $i = 1, 2$, is known [12] to greatly "enhance noise"; meaning that the deconvoluted signals are much noisier than the experimental signals. This numerical artifact has been controlled by means of a finite impulse response filter, implemented via the Parks-McClellan algorithm [13], with *optimal* low-pass band inspired in the Wiener approach (Ref. [14], Section 13.3). Namely, by setting its width to a few times (1–5) that frequency at which the power spectrum of the input signal drops by three orders of magnitude from the zero frequency level. The interval to the stop band is set to 0.05–0.2 times the sampling frequency, and the number of taps is set around 105. This smoothing is applied to the raw input data, and after each deconvolution operation.

Recognizing the danger of loosing peak sharpness with these smoothing operations, the specific parameters for each operation are set by monitoring the ratio of peak height to full width at half maximum (FWHM), after deconvolution, to its value in the input data. This ratio is raised by deconvolution, and it drops slightly with the degree of smoothing. By inspection, a limit of 1% drop, from the least smoothed, workable, curve, has been imposed to the smoothing parameters, a criterion which leads to a negligible effect on the ensuing fit parameters.

3.2. Modeling the tritium release

The T generated during neutron irradiation is approximately uniformly distributed throughout the bulk of the pebbles. Thus, its release is controlled mostly by the slower of either the surface desorption or diffusion processes. Considering the partially porous materials used in this study, the ceramic grains will be considered as the relevant "bulk" structures, for the diffusion control model.

The tests of surface desorption (SD) have assumed the Redhead [15] model, as described in Section 2 of Avila [16] This model proposes the evolution of the coverage (fraction of surface desorption sites occupied) remaining by time t, as:

$$\frac{df}{dt} = -k_s(t)f^n, \tag{7}$$

where n is the desorption order, and $k_s(t)$ is the temperature-activated release coefficient, of the form

$$k_s(t) = k_{os}\exp(-E_{as}/k_BT), \tag{8}$$

where, k_{os} is the pre-exponential factor, E_{as} is the activation energy, k_B is the Boltzmann constant, and T is the absolute temperature.

Similarly, if the T release is controlled by diffusion, the relevant magnitude is the diffusion coefficient, $D(t)$. Assuming that $D(t)$ is concentration independent, and given as in the expression (8), with k_{ob} and E_{ab} in place of k_{os} and E_{as}, it has been shown [17] that an Arrhenius analysis is possible, from which k_{ob} and E_{ab} are obtained.

The Arrhenius analysis, of either the SD or BLR models, assumes the whole release curve is the result of a single release mechanism, an assumption rarely met, in practice. For more complex processes a Marquardt–Levenberg non-linear least-squares (NLLS) procedure is applied.

Both, the Arrhenius and NLLS analyses will disregard the possible surface coverage (or bulk density), and temperature dependences of the activation energy and pre-exponential factors of the surface desorption and bulk diffusion coefficients. This choice is acknowledged as unavoidable, considering the lack of any reasonable estimate of the tritium surface coverage, or bulk density of trapping sites. In so doing, any dependence on those parameters will appear as an artificial correlation between $\mathrm{Log}(k_o)$ and E_a of the model being analyzed, a behavior known as the *compensation effect* [18].

A measure of the goodness of fit is necessary for comparison of the various BLR or SD model sets which may result in similar error

curves (values of the fit minus values of the deconvoluted release curve). This measure should be rather independent of the level of smoothing applied after the deconvolution operation, which is not the case of the customary standard error of the estimate (SEE) (square root o the (sum of squares of the errors, divided by (the number of points, minus the number of variables, minus 1))). An illustration in this regard is given with Fig. 9, below.

To avoid that dependency, and for comparing the fits of one release experiment to another, the number of points over the relevant temperature range (1–99% of the total release) will be set to 1000, by down-sampling interpolation within the measured trace, and each experimental trace will be *normalized* (and rendered adimentional), by dividing by the release maximum. Then, the low frequency error power (LFEP) will be used as a measure of the error, by averaging the power spectrum of the error from the lowest frequency of 10^{-3} to $8{\cdot}10^{-3}$. This measure includes oscillations of the error with up to eight cycles over that relevant temperature range, a number that is expected to weigh the error incurred by missing release peaks.

4. Results and analysis

4.1. Effect of pebble support during irradiation

Early practice within the present research was to irradiate the ceramic pebbles in evacuated quartz ampoules, which were supported in loosely fit aluminum foil into the aluminum canisters which go into the moderating-cooling water of the RECH-1 reactor. Then, it was noticed that, in some T release experiments, a T spike would be revealed by the ionization chambers, immediately upon breaking the ampoules, at room temperature. Suspecting that some T had been released from the ceramic into the ampoule during irradiation, tests have been made with Li_2TiO_3 pebbles, either maximizing or minimizing their heat release during that stage. Thus, in one set of samples, cooling was minimized by holding the evacuated ampoules in loosely fit alumina, into the canisters. In another set, cooling was maximized by back-filling the evacuated ampoules with He, at atmospheric pressure, before sealing, and supporting the ampoules in tightly fit graphite, which fits tightly to the aluminum canisters. The two sets of samples will be called *non-temperature moderated*, and *temperature moderated*, respectively.

Fig. 3 shows the T released from a non-temperature moderated capsule (these data have not been deconvoluted, as the procedure is unstable at the extremes of the time range, especially for sharply varying data). Immediately upon breaking the ampoule, a sharp release peak is reported by both ionization chambers. The signal from IC-1 (I_1) is slightly larger than that from IC-2 (I_2), indicating a mixture of oxidized and non-oxidized T. During the temperature

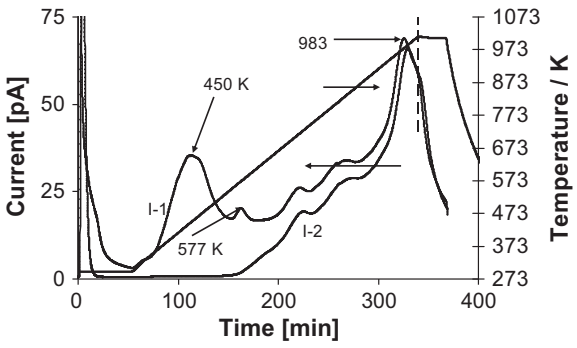

Fig. 3. Tritium release, at 2.5 K/min, from Li_2TiO_3 pebbles irradiated in an evacuated ampoule, which was supported in alumina.

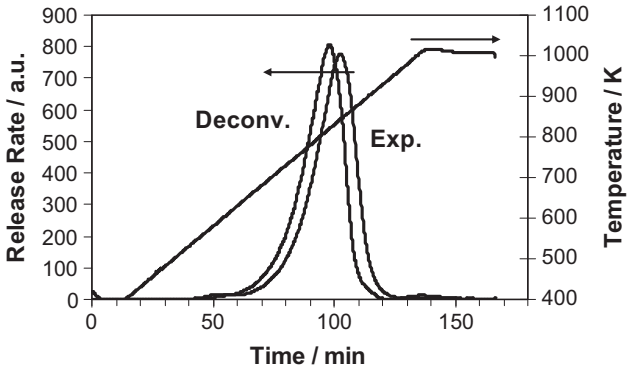

Fig. 4. Effect of deconvolution of the non-oxidized T signal from Li_2ZrO_3, taken at 5 K/min.

ramp, started 50 min after breaking the ampoule, T is released in oxidized form up to ~550 K, as revealed by the structure of I_1 while I_2 is negligible. At higher temperature, a shift occurs towards release in the non-oxidized form, reaching a peak near 980 K, where I_1 is only a few percent higher than I_2.

In comparison, T release from the temperature moderated ampoules appears as shown in Fig. 5, below, with a minimal release immediately upon breaking the ampoule, at room temperature, and a broad release peak during the temperature ramp. The suggestion is that in the non-temperature moderated capsules the temperature may have reached well above 700 K, during irradiation. Thus, the gradual rise of I_1 and I_2 from ~600 to 980 K is due to residual T not released to the interior of the capsule during irradiation, or reabsorbed into the ceramic upon extraction from the reactor core.

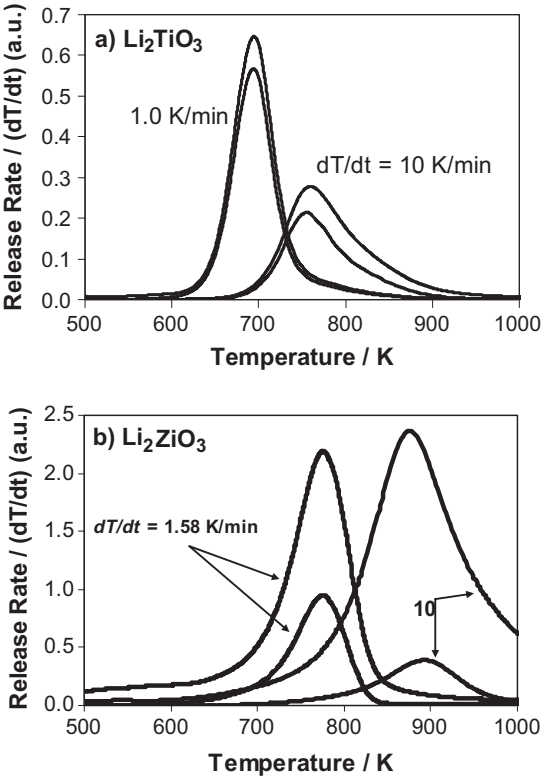

Fig. 5. Tritium release from (a) Li_2TiO_3 and (b) Li_2ZrO_3 divided by the temperature ramp rate. In each pair, the higher curve corresponds to IC-1, and the lower one to IC-2.

Thus, back-filling the quartz ampoules with He and a graphite capsule-to-canister support appear as an effective heat transport path out of the Li-ceramic pebbles during in-core irradiation. The experiments reported next were conducted using the temperature moderated assemblage.

4.2. Effect of tritium signal deconvolution

The release of T from several ampoules filled with either lithium titanate or lithium zirconate, prepared and irradiated as described above, was carried out at heating rates from 1 to 10 K/min. T release from Li_2TiO_3 at temperature ramp rates of 1 (two experiments), 2.5, 5 (two experiments), and 10 K/min will be analyzed first, in the Arrhenius representation, considering the whole release data. Then, parameter fitting will be applied over the most relevant range by the NLLS procedure.

The effect of deconvoluting the T release signal from the response of the analysis system is shown in Fig. 4. As compared to the original experimental signal, the deconvoluted curve moves to lower temperature, in this case, by 4.3 K, and the peak sharpness (ratio of maximum to FWHM) increases by 8.6%.

Typical T signals are shown, after deconvolution, in Fig. 5. The relation of the non-oxidized to the oxidized signals varies significantly, an effect thought to derive from incomplete drying of the pellets before sealing the quartz ampoules for irradiation.

4.3. Surface desorption analysis of tritium from Li_2TiO_3

4.3.1. Analysis of the non-oxidized signal

The analysis of the non-oxidized (IC-2) signal is presented, next, to be followed by the analysis the oxidized T signal, given by the difference from the IC-2 to the IC-1 signals.

4.3.2. Arrhenius analysis

The IC-2 traces have been analyzed according to bulk limited release (BLR), and first order (SD1) and second order (SD2) surface desorption models, as shown in Fig. 6. In the comparison of the three release models, the SD2 traces are closest to straight lines, pointing to this mechanism as the main hindrance in the release of non-oxidized T. Thus, this model is applied, also, to other release experiments, resulting in the traces shown in Fig. 7.

From the latter figure, the average value of $E_a = 241 \pm 19$ kJ/mol, and the logarithmic average of $f_o k_{os} = 4.7 \cdot 10^{14}$/s (with uncertainty

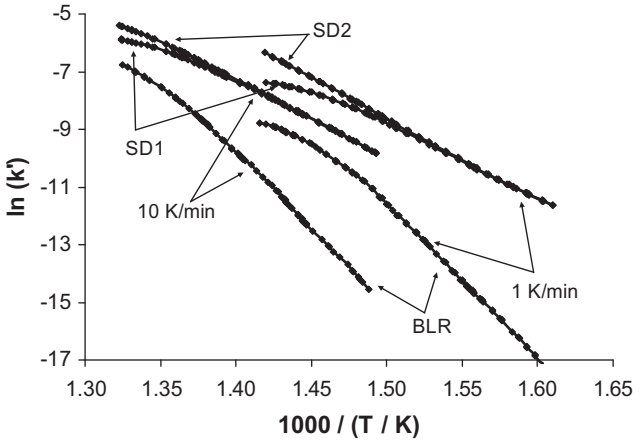

Fig. 6. Arrhenius analysis of the non-oxidized T release from Li_2TiO_3. For each ramp rate, the SD1 and SD2 analyses coincide at low temperature, and SD1 deviates to lower values at higher temperature. Both BLR analyses deviate similarly to the SD1 analyses from a linear relation. (k' is $f_o k_s(T)\cdot s$ for the SD models, and $D(T)/(cm^2/s)$ for BLR).

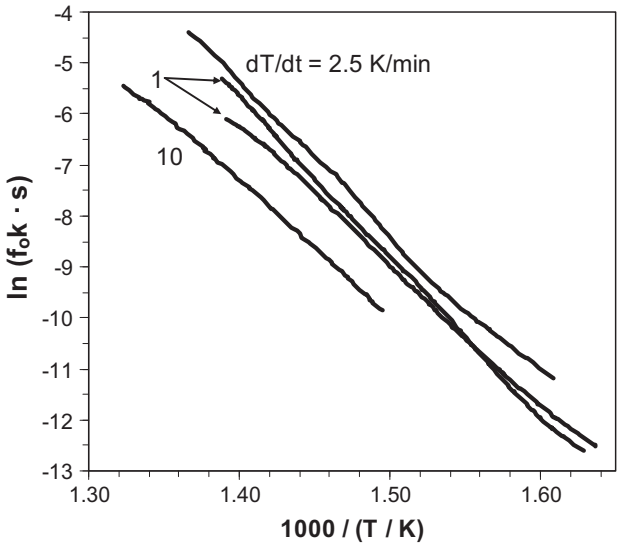

Fig. 7. Arrhenius representation of second order surface desorption model of the non-oxidized trace of tritium release from Li_2TiO_3.

of a factor of 50). These values imply a temperature for a residence time of 1 day ($T_{1dRres} = (E_a/k_B)/\ln(\tau k_o f^{m-1})$, at $\tau = 1$ day) of 630 K; the latter, assuming $f_o = 1$, i.e. total coverage of the T adsorption sites. Lacking knowledge of f_o, the pre-exponential factor, k_{os}, usually interpreted as the attempt-to-escape frequency, cannot be inferred.

4.3.3. Non-linear least-squares analysis

The NLLS procedure has been applied to fit the non-oxidized T release from Li_2TiO_3. As expected from the Arrhenius analysis, a single SD2 model fits the release curves at ramp rates of 1–5 K/min, over most of the peak range. However, in addition to that main signal, a stretching is observed towards the end of the temperature scan, well beyond the trailing edge of the SD2 peak. The possibility of tritium being retained by the ionization chambers, for slow later release (memory effect), has been ruled out by the sharp drop of the respective signals upon cooling of the furnace. Attempts at fitting a second SD model in that *stretching* region lead mostly to unconvincing values of the kinetic parameters, suggesting that the stretching is not caused by a single release mechanism. In only one case, at the faster ramp rate, of 10 K/min, a rather reasonable second SD2 process does fit the high temperature stretching, as shown in Fig. 9, below.

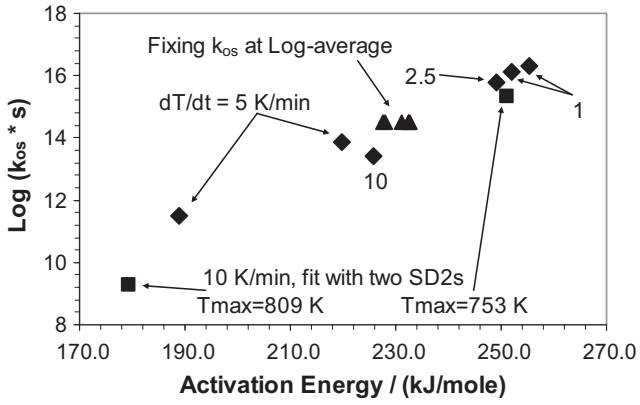

Fig. 8. Kinetics of the second order desorption model, on non-oxidized tritium release from Li_2TiO_3.

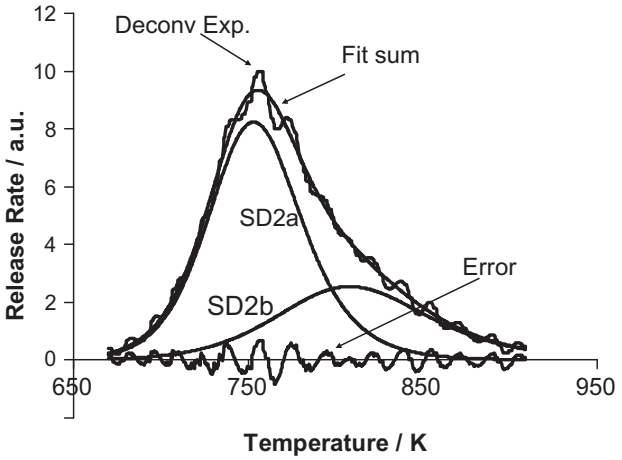

Fig. 9. NLLS analysis with 2 s order desorption processes of the trace of non-oxidized tritium release from Li_2TiO_3 at ramp rate of 10 K/min.

To stay away from the high temperature stretching, the kinetic parameters of the single SD2 process have been fit, with the NLLS procedure, to the peak range starting at ~1% of the total release, and up to half of the maximum release rate, past the peak, thus encompassing ~77% of the total release. Lacking information on the degree of initial coverage, f_o, of the T adsorption sites, this value has been set to one, while the overall scale of the SD2 trace is fixed to match its integral value to that of the experimental trace over the temperature range under analysis. Thus, only E_{as}, and Log(k_{os}) are adjusted by the NLLS procedure. A summary of the resulting kinetic parameters is shown in Fig. 8.

In the figure, the diamonds represent the fit with just one SD2 process for each of the six release curves. In addition, the fit shown in Fig. 9, to be described, below, is represented by squares, and identified by the label at the bottom of the figure.

The average values of E_{as}, 241 ± 29 kJ/mol, and Log(k_{os}), 15.1 ± 2, are essentially the same as those from the Arrhenius analysis. The more robust parameter, T_{1dRres}, which is rather independent of the shape of the release peak, has the average value of 620 ± 15 K, where the standard deviation is 27% of the typical FWHM in a ramp at 1 K/min (of which the maximum occurs at 687 K). This rather narrow spread of T_{1dRres} suggests that, irrespective of the temperature ramp rate, the data relate to the same desorption process.

A strong *compensation effect*, i.e. the close to linear relation (correlation factor $R^2 = 0.97$, among the values represented by diamonds) of Log(k_{os}) to E_{as}, is evident in Fig. 8, over the E_{as} range of ~190 to 260 kJ/mole. A measure of the agreement between the various results in that figure can be had by fixing Log(k_{os}) at its average value (from the data represented by diamonds in that figure), and fitting the release curves by adjusting E_{as}, only. The spread of the resulting E_{as} values, represented by the triangles in Fig. 8 is much narrower. A certain additional correlation (at factor $R^2 = 0.64$) is observed, of Log(k_{os}), or E_{as}, vs. the TPD ramp rate, for which no mechanism has been identified.

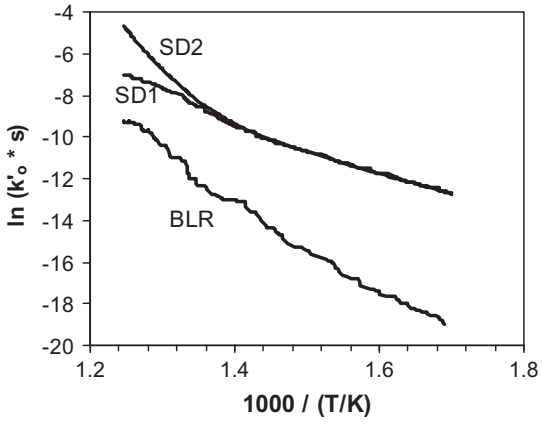

Fig. 10. Arrhenius analysis for testing surface desorption and BLR models of the non-oxidized trace of tritium release from Li_2ZrO_3, at ramp rate of 1.6 K/min (k', as in Fig. 6).

In SD1 or SD2 processes, for a given value of T_{max}, the higher values of E_{as}, with concomitant higher values of Log(k_{os}), result in sharper release peaks. Then, considering that the originally measured curve is stretched by the convolution of the TPD release at the furnace with the measurement system response, the error incurred in by analyzing the data without deconvolution has been tested, again within the SD2 model. The result is lower values of Log(k_{os}) and E_{as}, and a doubling of the compensation effect, as compared to the results in Fig. 8. For example, the compounded effect on the two parameters, with the data from the two experiments at 5 K/min, is a shift of T_{1dRres} from 604 K (using deconvoluted data), up to 622 K (without deconvolution). This shift is close to linear in the TPD ramp rate, so, it may be considered negligible for ramp rates of 1 K/min or lower, such that the deconvolution operation may not be necessary.

In the 10 K/min experiment (Fig. 9), the stretching of the peak towards higher temperature, mentioned, above, begins early during the trailing edge of the peak. In this case, the fit with two release processes is shown in the figure, with components SD2a and SD2b which peak at 753 and 809 K, and amount to 66% and 33%, respectively, of the total release. For this analysis, the initial coverage, f_o, of each process has been relaxed from unity, letting it represent the proportion of the respective contribution to the total release. The smoothing after deconvolution has been restrained, for this figure, to illustrate the shape of the error curve, and the different behavior of the standard error of the estimate (SEE), and the low frequency (up to a frequency of $8{\cdot}10^{-3}$) error power average (LFEP). These values are $2.6{\cdot}10^{-2}$, and $2.2{\cdot}10^{-6}$, respectively. A more aggressive smoothing (no noticeable *wiggles* in the deconvoluted curve) leads to essentially identical SD2 components, with values of SEE of $5.8{\cdot}10^{-3}$ and LFEP of $2.1{\cdot}10^{-6}$, showing the advantage of the LFEP as a rather smoothing-independent measure of the error.

4.3.4. Analysis of the oxidized T signal

The oxidized T signal is calculated as the difference from the IC-2 to the IC-1 signals. Being the difference between two signals, which are close in several experiments, the oxidized T release curves are more irregular than those of the non-oxidized signal. Thus, consistent fits have been possible only to experiments at ramp rates of 1, 5 (2 experiments), and 10 K/min. Again, the SD2 model provides the best fits, leading to, on average, a main release peak, involving ~62% of the total release, at $E_{as} = 172$ kJ/mole, $k_{os} = 5.5{\cdot}10^9$/s ($T_{1dRes} = 611$ K), and a higher temperature process, which releases ~25% of the total at $E_{as} = 192$ kJ/mole, $k_{os} = 9{\cdot}10^9$/s ($T_{1dRes} = 674$ K).

4.4. Surface desorption vs. bulk diffusion limited release of tritium from Li_2ZrO_3

The TPD release of T from Li_2ZrO_3 shares its major features with that from Li_2TiO_3. However, in this case, the Arrhenius analysis shows that the SD2 model does not apply; rather, the SD1 and BLR models achieve closer fits. A typical comparison of these models is shown in Fig. 10.

In the comparison of the three release models shown in Fig. 10, the BLR and SD1 traces are closer to straight lines than the SD2

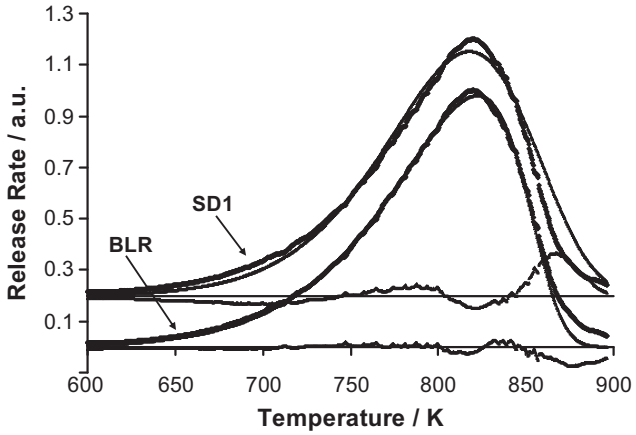

Fig. 11. BLR and SD1 NLLS analysis, up to half height past the release maximum, of the IC-2 trace of tritium release from Li_2ZrO_3 at ramp rate of 5 K/min. The SD1 fit is displaced upwards, for clarity. In each set of curves the thick curve is the experimental data, the thin curve is the model fit, and the lower trace is the error.

trace, even though systematic deviations are apparent in both the BLR and SD1 analyses. This nonconformity to either release model may be caused by a superposition of models which may invalidate the Arrhenius analysis.

To reduce the effect of those possible superpositions, the more flexible NLLS procedure has been applied, with the BLR and SD1 models, as in the case of Li_2TiO_3, over the peak range from ~1% of the total release, and up to a release rate of half past the maximum. In this case, this range covers ~88% of the total release.

The NLLS procedure fits the non-oxidized T data with better LFEP using the BLR model, than it does with the SD1 model, by an average factor of 4. Admitting that this error difference is small, these experiments alone are insufficient to ascribe the control of T release from Li_2ZrO_3 to either bulk diffusion or surface desorption. As an example of the quality of the data fits, the best BLR fit (LFEP = $8.7\cdot10^{-6}$), and corresponding SD1 fit (LFEP = $1.25\cdot10^{-4}$), are shown in Fig. 11. In only one case (at ramp rate of 2.5 K/min), is the SD1 fit slightly better than that of the BLR model, and in that case, both at higher LFEP values of $3.8\cdot10^{-5}$, and $6.9\cdot10^{-5}$, respectively.

The kinetic parameters of SD1 and BRL fits to data from TPD experiments performed at 1, 1.6 (two experiments), 2.5 (two experiments), 5, 7, and 10 K/min are summarized in Fig. 12.

As in the case of the SD2 analysis of release from Li_2TiO_3, a pronounced *compensation effect* is evident in both types of analysis of the Li_2ZrO_3 data. Concentrating on average values, the activation energy averages are 154 ± 19 kJ/mole in the SD1 model, and 260 ± 27 kJ/mole, in the BLR model. The corresponding logarithmic averages of the pre-exponential factors are $2.7\cdot10^6$/s, with uncertainty of a factor of 11, and $4.1\cdot10^6$ cm^2/s, with uncertainty of a factor of 50.

The calculated kinetic parameters imply the temperatures for a residence time (given by $b^2/(15D(T))$ within the BLR model) of 1 day (T_{1dRes}) of 661 ± 17 K, according to the SD1 model, and $T_{1dRes\text{-}BLR}$ = 735 ± 17 K within the BLR model (cf. ~580 to 682 K within the diffusion model, in Fig. 31 of the 1993 *ITER Solid Breeder Blanket Materials Database* [19]). If the BLR model is applicable to the data, the value calculated for $T_{1dRes\text{-}BLR}$, which is substantially higher than the reference values in the *Database*, may be an indication that the release is hindered by other processes, such as surface desorption, in addition to diffusion within the ceramic grains. (In this regard, the uncertainty in the assumed grain size does not affect the value of $T_{1dRes\text{-}BLR}$, since, given an experimental release curve, the fitted diffusion coefficient, $D(T)$, is proportional to b^2). On the contrary, within the usual interpretation of the pre-exponential factor, k_{os}, of the SD1 model as an attempt-to-escape frequency, the values displayed in Fig. 12 are unexpectedly low; an indication that the SD1 model may not apply to the data.

The oxidized T release from Li_2ZrO_3 has been analyzed, also, with the NLLS procedure. Noting a peak or early rise shoulder in the main peak, around 600 K, a bold multy peak fit has been attempted for the data from a ramp at 5 K/min, as shown in Fig. 13. For this case, again, the initial coverage, f_o, of each process has been relaxed from unity. The major features of the fit are a main release peak preceded by one or more shallow structures, and going into a not resolved process at the high temperature end. Here, similarly as with the non-oxidized signal, the main peak is fit mostly by an SD1 model, with E_{as} = 130 kJ/mole, and Log(k_{os}) = 5.7, leading to T_{1dRes} = 646 K. The low and high temperature shoulders can be accounted for with, mostly, SD1 or SD2 models. In addition, major model changes, like an SD2 main peak, are possible, with concurrent reshaping of the adjacent components, leading to little degradation of the fit quality (factors of two higher LFEP). With similar degradation, a BLR processes (which would require some clear justification) may replace the lower temperature SD1, but not the other structures. These variations on the data fitting theme are indicative of the large uncertainty associated to these procedures. Still, the bold suggestion is made that the low temperature SD2 process would correspond to surface desorption of T which was at, or very near the surface, before initiating the temperature ramp, in the form of water, carrying a surface oxygen

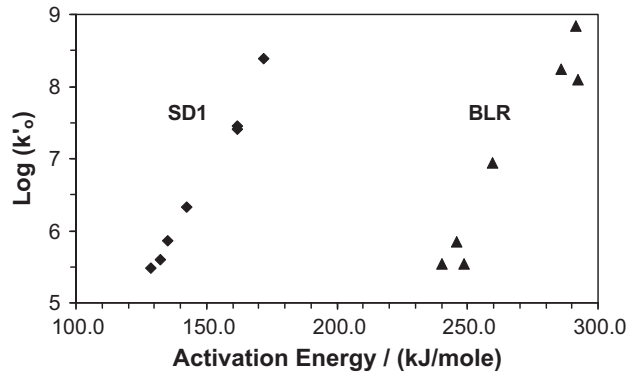

Fig. 12. Kinetic parameters of BLR and SD1 NLLS analysis of non-oxidized tritium release from Li_2ZrO_3 at ramp rate of 5 K/min (k'_o is k_{os}·s, in the SD1 model, and k_{ob}/(cm^2/s) in the BLR model).

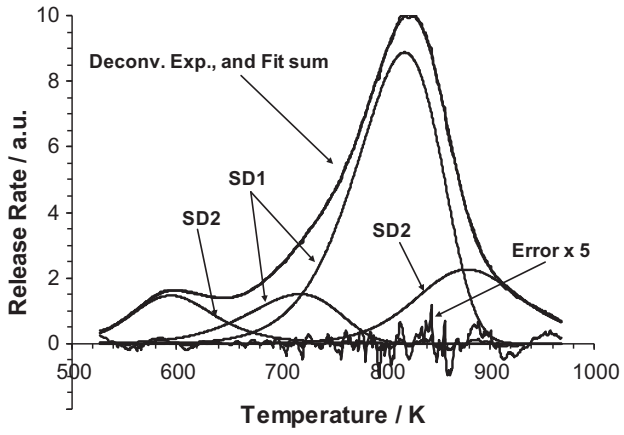

Fig. 13. Multy desorption process analysis of the oxidized trace of tritium release from Li_2ZrO_3.

with it. The higher temperature processes would correspond to T being released from deeper in the ceramic grains, or the pebbles.

5. Discussion

A first word of caution is in order, as regards the comparison of the present batch release experiments to in-core, continuous irradiation and release experiments (especially so if the latter are carried out in a high flux reactor), or to its relevance to the behavior of these ceramics in a future fusion reactor first wall. The main contrast is the concomitant high level of gamma and neutron irradiation, which, most certainly, will raise the diffusion rate, and facilitate the release of T from trapping sites. In addition, the calculated values of ^{6}Li burn-up, and dpa (Section 2), are well below the values expected within a fusion reactor first wall, or recently achieved within high flux fusion reactor in-core experiments.

As stated in the Section 1, the detailed processes leading to the release of T may be much more complex than just the formation of tritiated H_2 or H_2O. In this regard, Oyaidzu et al. [7] have proposed that T release from Li_2ZrO_3 is related to the annihilation of the E', oxygen vacancy centers, which appear to conform to first order kinetics. However, the corresponding activation energies, of 77 kJ/mole for E' annihilation, is far from the value of 154 kJ/mole, calculated in this work for T release within the SD1 model.

The contrast of BLR or SD1 behavior in Li_2ZrO_3, against SD2 behavior in Li_2TiO_3 may be related to the larger grain size in the former material. Bertone [20] has shown that the quantity which favors BLR over SD1 release, is

$$\beta = b\frac{k_{os}}{k_{ob}}\exp((E_{ab} - E_{as})/k_BT), \tag{9}$$

where b is the ceramic grain radius. A value of $\beta < 1$ implies that the main hindrance to release is surface desorption, while $\beta > 10$ implies that bulk diffusion is the limiting process. These values follow from the release equations under simultaneous diffusion and first order desorption control. The inspection by the present authors of the case of diffusion coupled to second order desorption suggests that it may be not solvable in closed form, since, in this case, the problem is not of the Sturm–Liouville type, leading to elementary solutions which are not orthogonal. However, the parameter β is still a good measure of the relative hindrance to release afforded by either diffusion or desorption.

So, understanding the contrast of BLR or SD1 behavior in Li_2ZrO_3, vs. SD2 behavior in Li_2TiO_3 would require the surface desorption and bulk diffusion coefficients of both materials. Within that assessment, the roughly factor of three difference of the grain size from the Li_2TiO_3 to the Li_2ZrO_3 ceramics does not justify the clear distinction of the release behavior from these materials. Certainly, significant quantitative, if not qualitative, differences must exist between the respective chemical processes of tritium trapping and diffusion among the two materials.

Acknowledgments

This work has benefited from the expert advise of Dr. Carl E. Johnson, of the *Argonne National Laboratory*, Argonne, IL, USA, under the auspices of the IAEA. We are indebted to Dr. Masabumi Nishikawa of the Graduate School of Engineering Science, Kyushu University, Japan, has provided the Li_2ZrO_3 pellets (from Cerac Inc., USA) used in this study. The support for personnel training and equipment from IAEA is gratefully acknowledged.

References

[1] C.E. Johnson, K. Noda, N. Roux, J. Nucl. Mater. 258–263 (1998) 140.
[2] R. Lässer et al., Tritium in Fusion: R&D in the EU, in: Tritium Science and Technology Conference, Rochester, 16 September 2007.
[3] O.D. Slagle, T. Kurasawa, R.A. Verrall, G.W. Hollenberg, In situ tritium recovery from Li_2O and Li_2ZrO_3 irradiated in a fast neutron flux: BEATRIX-II, phase I and II, in: C.E. Johnson (Ed.), CBBI-III, Univ. of California at los Angeles, Argonne Natl. Lab., Argonne, Illinois, USA, 22–24 June 1994, p. 175.
[4] S. Casadio, J.G. van der Laan, C. Alvani, A.J. Magielsen, M.P. Stijkel, J. Nucl. Mater. 329-333 (2004) 1252–1255.
[5] J. Mougin, B. Rasneur, N. Roux, Tritium and helium release from Li_2TiO_3 comparison with Li_2ZrO_3, in: Proc. 3rd Inter. Workshop on Ceramic Breeder Blanket Interactions, Los Angels, 1994, p. 227.
[6] G. Federici, A.R. Raffray, M.A. Abdou, J. Nucl. Mater. 173 (1990) 185–213.
[7] M. Oyaidzu, H. Kimura, A. Yoshikawa, Y. Nishikawa, K. Munakata, M. Okada, M. Nishikawa, K. Okuno, Fusion Eng. Des. 81 (2006) 583–588.
[8] C. Alvani, P. Ccarconi, S. Casadio, V. Contini, A. Dibartolomeo, F. Pierdominici, A. Depatula, S. Lagos, C. Nannetti, J. Nucl. Mater. 289 (2001) 303.
[9] S. Casadio, J.G. van der Laan, C. Alvani, A.J. Magielsen, M.P. Stijkel, J. Nucl. Mater. 329-333 (2004) 1252.
[10] J.F. Ziegler, The Stopping and Range of Ions in Matter: SRIM, 2008. <http://www.srim.org/>.
[11] R.A. Verral, J.M. Miller, S.R. Bokwa, Adv. Ceram. 25 (1989) 41.
[12] Normand Beaudoin, Fourier transform deconvolution of noisy signals and partial Savitzky–Golay filtering in the transformed side, in: Proceedings of Vision Interface, 1999. <http://www.gel.ulaval.ca/~parizeau/vi99/Proceedings/node107.html#1734>.
[13] A.V. Oppenheim, R.W. Schafer, Discrete-time Signal Processing, Prentice Hall, 1989 (Sec. 7.6. Numerical Implementation Taken from the National Istruments LabView library (v. 8.0 (2005), <www.ni.com>)).
[14] Numerical Recipes in Fortran 77: The Art Of Scientific Computing, Cambridge University Press, 1992.
[15] P.A. Redhead, Vacuum 12 (1962) 203.
[16] R.E. Avila, Jpn. J. Appl. Phys. 45 (2006) 9254.
[17] R.E. Avila, Jpn. J. Appl. Phys. 43 (2004) 7205.
[18] D.L.S. Nieskens, A.P. van Bavel, J.W. Niemantsverdriet, Surf. Sci. 546 (2003) 159–169.
[19] M.C. Billone, W. Dienst, T. Flament, P. Lorenzetto, K. Noda, N. Roux, ITER Solid Breeder Blanket Materials Database, Argonne National Laboratory, Rep. ANL/FPP/TM-263, 1993 (Fig. 31).
[20] P. Bertone, J. Nucl. Mater. 151 (1988) 281.